Advances in Science and Technology Research Journal

Advances in Science and Technology Research Journal, 2026, 20(9), 40–60
https://doi.org/10.12913/22998624/222235
ISSN 2299-8624, License CC-BY 4.0

Received: 2026.04.16
Accepted: 2026.07.10
Published: 2026.08.01

Evaluation of high-performance concrete properties with partial replacement of glass powder, ultra-fine glass powder, and waste low-density polyethylene beads

Mahmoud Abdelsalam Aref Obeid[1*], Mohammed Ibrahim Abu-Mahadi[1], Alexey Semenovich Markovich[1,2], Qais Abdulrahman Ali Qais[1], Ekaterina Borisovna Markova[3]

[1] Department of Construction Technologies and Structural Materials, RUDN University, 6 Miklukho-Maklaya St., Moscow 117198, Russian Federation
[2] Department of Metal and Timber Structures, Moscow State University of Civil Engineering (National Research University), 26 Yaroslavskoye Shosse, Moscow 129337, Russian Federation
[3] Department of Physical and Colloidal Chemistry, RUDN University, 6 Miklukho-Maklaya St., Moscow 117198, Russian Federation
[*] Corresponding author's e-mail: mahmoud.obeid@yandex.com

ABSTRACT

The construction industry generates vast quantities of non-biodegradable waste, such as glass cullet and plastic scraps, posing serious environmental challenges that require innovative recycling strategies in concrete production. This study evaluates the mechanical and physical properties of high-performance concrete incorporating glass powder (GP) and ultra-fine glass powder (UFGP) as partial replacements for fine aggregate, together with low-density polyethylene (LDPE) granules as a partial substitute for coarse aggregate, using locally available quartz-based materials. Ten distinct concrete mix designs were prepared using ordinary Portland cement (OPC) Grade 53, fractionated quartz sand, and crushed vein quartz as coarse aggregate. GP and UFGP replacement levels ranged from 0% to 20%, while LDPE replacement levels varied from 0% to 15%. All specimens were cured for 28 days and subsequently tested for compressive strength, water absorption, ultrasonic pulse velocity (UPV), modulus of elasticity, and density. The results showed that the mix containing 10% GP and UFGP replacement (Mix B) achieved the highest compressive strength of 61.98 MPa, representing a 10.9% improvement over the control mix, which recorded 55.91 MPa. The hybrid mix (Mix E), incorporating 10% GP and UFGP together with 5% LDPE, attained a compressive strength of 57.38 MPa while reducing the specimen weight to 2425.95 g and achieving the lowest water absorption rate of 0.54%. However, increasing the LDPE content beyond 10% resulted in significant strength deterioration; for example, Mix K, containing 15% LDPE, recorded a compressive strength of only 29.16 MPa. The incorporation of GP and UFGP improved workability, as indicated by slump values increasing from 45 mm to 210 mm. Conversely, the addition of LDPE gradually reduced the modulus of elasticity from 37 GPa to 25 GPa. Ultrasonic pulse velocity measurements of 5.51 km/s for Mix B confirmed that GP and UFGP enhanced concrete density and internal compactness, whereas the inclusion of LDPE adversely affected internal homogeneity. These findings suggest that optimal combinations of GP, UFGP, and low percentages of LDPE can produce sustainable lightweight concrete suitable for structural applications, effectively diverting waste materials from landfills while maintaining acceptable mechanical performance and durability.

Keywords: high performance concrete, low-density polyethylene, glass powder, ultra-fine glass powder, Python, quartz, silicon dioxide.

INTRODUCTION

The integration of industrial by-products and waste materials into cementitious composites represents a critical strategy for advancing sustainable construction. As the most widely consumed manufactured material globally, concrete provides a unique matrix for incorporating diverse waste materials while simultaneously enabling targeted modifications to its mechanical and physical properties. Among these alternatives, quartz-based materials such as quartz vein material and quartz sand have attracted considerable research interest as potential partial or full replacements for conventional aggregates. Although quartz is fundamentally composed of silicon dioxide (SiO_2), its performance within a cementitious matrix depends not only on chemical purity but also on physical characteristics such as particle size distribution, morphology, surface texture, and impurity content [1,2].

Several studies have reported that quartz sand can provide beneficial or acceptable performance in concrete applications. For example, the incorporation of white quartz sand has been shown to improve mechanical properties and enhance durability characteristics, including reduced chloride ion permeability and lower water absorption [3,4]. One study reported that replacing 5% and 10% of fine aggregate with quartz sand in non-air-entrained concrete produced acceptable results, with compressive strengths of 26.483 MPa, 26.087 MPa, and 23.824 MPa for the 5% quartz, control, and 10% quartz mixtures, respectively [5].

In contrast to the variable performance of quartz additives, glass powder (GP) and its ultrafine variant (UFGP) have been consistently identified as effective supplementary cementitious materials (SCMs) capable of enhancing the mechanical properties of concrete, particularly compressive strength. The incorporation of GP utilizes the pozzolanic reaction, in which the amorphous silica present in glass reacts with calcium hydroxide (portlandite), a by-product of cement hydration, to produce additional calcium silicate hydrate (C-S-H) gel [6,7]. Studies have demonstrated that partial cement replacement with GP can produce favorable outcomes. For instance, replacement levels of up to 10% have been shown to improve strength while reducing drying shrinkage [8]. More substantial improvements have been reported at higher replacement levels. One study achieved a maximum compressive strength of 47.5 MPa by combining 15% recycled glass powder (RGP) with 1% nano-silica (NS) as cement replacement materials [9], while another investigation reported that a 25% glass powder replacement achieved a compressive strength of 115 MPa at 7 days, demonstrating its potential for high-strength and reactive powder concrete (RPC) applications [10]. The particle size of glass powder is a critical parameter governing its reactivity and, consequently, its influence on concrete performance. This distinction has led to the classification of ultrafine glass powder (UFGP) as a separate category. UFGP offers distinct advantages over micro-sized glass powder, particularly in accelerating early-age strength development. Lam [11] reported that UFGP increased the compressive strength of cement paste by 50% after 1 day and by 5% after 28 days. This accelerated reaction is primarily attributed to the significantly larger specific surface area of ultrafine particles, which provides more active sites for the pozzolanic reaction and enhances early cement hydration. Overall, GP—and especially UFGP—provides a practical approach for tailoring the mechanical properties of concrete. In addition, the partial replacement of Portland cement with these materials contributes to reducing the environmental impact associated with cement production while simultaneously improving long-term strength and durability.

Along with mineral additives, the incorporation of low-density polyethylene (LDPE) granules or fibers into concrete provides an effective approach for producing lightweight, high-performance composites. Unlike mineral additives, LDPE possesses unique physical characteristics that significantly reduce the density of concrete. As a result, the produced material becomes suitable for applications where reduced dead load and improved thermal insulation are important, such as partition walls, paving blocks, and protective barriers.

Although the inclusion of LDPE generally reduces compressive strength, it enhances the suitability of concrete for specialized non-structural and semi-structural applications. This approach enables engineers to optimize concrete not solely for maximum strength, but for a balanced combination of workability, durability, thermal performance, and functional efficiency [12].

Problem

Despite the promising attributes of individual additives, significant challenges remain in predicting and controlling the performance of quartz-modified concrete. A substantial body of research indicates that quartz incorporation may have a neutral or even negative effect on compressive strength. Previous studies have reported notable strength reductions when crushed quartz powder was added to concrete mixtures; for example, one investigation found that the inclusion of quartz powder reduced compressive strength by approximately 9.3% and 13.4% under different conditions[13]. These findings suggest that the physical form of the quartz additive—whether coarse and angular quartz vein material used as structural aggregate or finely ground quartz powder functioning as a filler or pozzolanic material—is a critical factor influencing performance. The effectiveness of quartz as a filler depends largely on its ability to achieve dense particle packing, which is governed by particle grading and fineness modulus [14].

The incorporation of polymeric inclusions such as low-density polyethylene (LDPE) introduces additional complexity to concrete behavior. Several studies have quantified the influence of plastic waste on compressive strength, demonstrating that replacing fine aggregate with plastic waste can reduce compressive strength by approximately 35% to 50% [15]. Similarly, one study reported reductions of 5%, 15%, and 30% in 28-day compressive strength with increasing proportions of recycled plastic aggregates [16].

Research gap

The conflicting findings regarding quartz additives suggest that their performance cannot be generalized, as it is governed by the physical form of the material and its engineered role within the overall aggregate gradation of the concrete mixture. Quartz may provide beneficial effects when functioning as a well-graded inert aggregate; however, it may become detrimental when acting as a poorly performing filler or when it disrupts optimal particle packing within the concrete matrix.

Furthermore, although the individual advantages of GP and UFGP have been extensively documented, and the lightweight potential of LDPE is well established, the existing literature lacks comprehensive investigations into the combined use of quartz sand, quartz stone, GP, UFGP, and LDPE within a single concrete system. In addition, despite the abundance of quartz resources in Jordan, their integrated application with recycled plastic waste in sustainable concrete formulations remains largely underexplored.

Objective

This study aims to develop and characterize sustainable concrete formulations incorporating quartz-based materials (quartz sand and quartz stone), GP, UFGP, and LDPE. The specific objectives are to evaluate the effects of these combined additives on compressive strength, microstructural density, and the overall performance of the concrete composite; to determine the optimal proportions that achieve a balance between lightweight characteristics and mechanical integrity; and to assess the suitability of the proposed formulations for construction applications utilizing locally available quartz resources and recycled plastic waste, particularly in Jordan.

MATERIALS AND METHODS

Materials

Every material used in this experimental study was carefully chosen.

- OPC Grade 53, according to the ASTM C114-85 standard.
- Fine aggregate, according to the ASTM C136-84. The sand has a high-purity fractionated quartz sand (≤4.75 mm) with a rounded particle shape and contains very few impurities with a moisture content of ≤0.2%, as shown in Figure 1. Table 1 shows a comparison of the chemical properties of quartz sand between Jordan and Russia.
- The coarse aggregate, well-graded crushed vein quartz (≤20 mm), which has the best packing density and particle properties. Its angular grains and rough, textured surface and its characteristics are shown in Figure 2.
- Low-density polyethylene (LDPE) plastic waste was processed into uniform 4–5 mm granules, as shown in Figure 3, so that they could be easily mixed in and used to strategically replace some of the aggregates in different mix designs.
- Micro glass beads, with two different size fractions (106–600 μm and 0–50 μm), were

added as a multifunctional additive to these materials to improve particle packing density and the interfacial transition zone, as shown in Figure 3.

- According to ASTM C187, the water-cement ratio (w/c = 0.38) and superplasticizer content (1.4%) were used. The mix design for all samples is shown in Table 2.

Methods

Specimen preparation

A total of 60 cubic specimens (100 × 100 × 100 mm) were prepared using ten distinct mix designs, with six replicates per mix to ensure statistical reliability.

Specimen preparation and curing

Fresh concrete mixtures were cast into steel molds in three equal layers, with each layer compacted by 25 blows using a standard tamping rod in accordance with ASTM C192/C192M. This procedure minimized air voids and ensured uniform density across all specimens. After casting, the specimens were covered and kept at an ambient temperature of 23 ± 2 °C for 24 hours. The specimens were then cured in water at 23 ± 2 °C for 28 days in accordance with ASTM C511.

Surface drying and evaluation preparation

After curing, specimens were surface-dried and then subjected to a multi-parameter evaluation protocol. Compressive strength testing was performed using a calibrated universal testing machine, complying with ASTM C39/C39M. Water absorption capacity was determined by measuring the mass difference between dried and saturated surface-dry conditions. Additionally, non-destructive ultrasonic pulse velocity

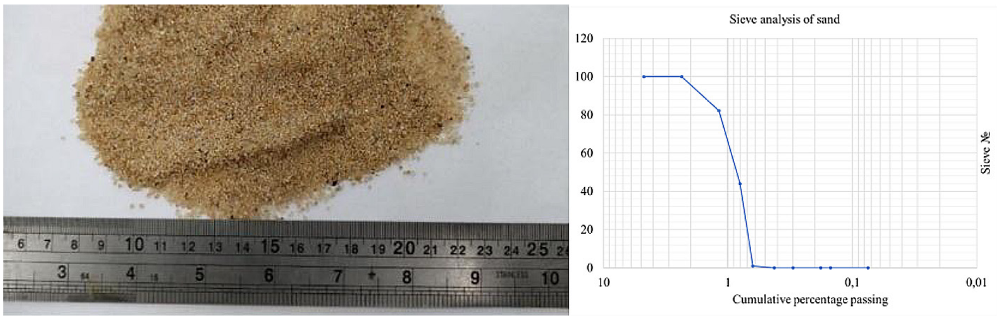

Figure 1. Sieve analysis of fractionated quartz sand

Table 1. Comparison of chemical properties of quartz sand

Chemical properties of quartz sand		
Major oxides	In Jordan (Ras En Naqb) Ministry of Energy and Mineral Resources [17]	In Russia (Crystal Mountain) [18]
SiO_2	98.7	98.9
Al_2O_3	0.52	0.62
Fe_2O_3	0.04	0.07
Na_2O+K_2O	0.11	0.105

Figure 2. Vein quartz was observed under a polarizing microscope (Altami Polar 3)

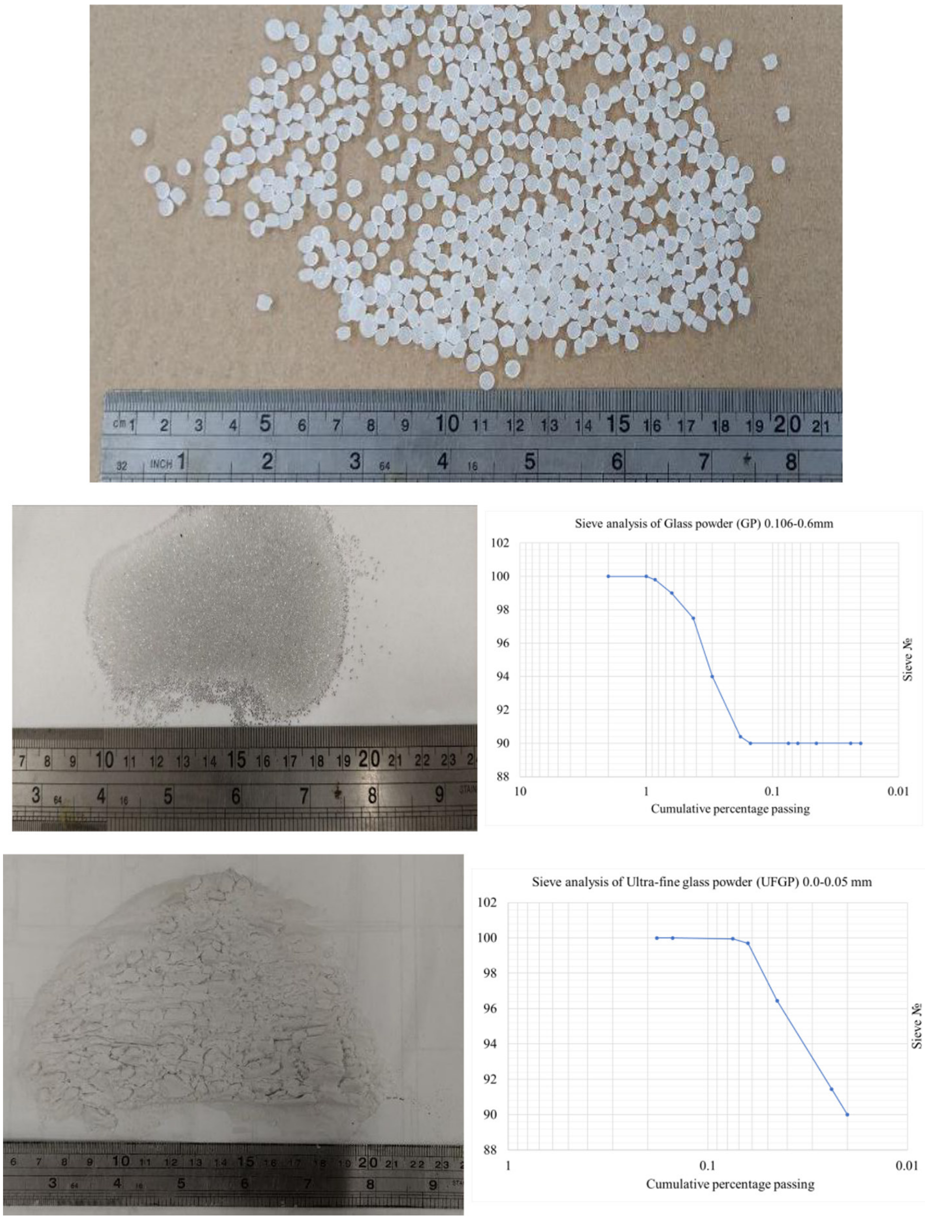

Figure 3. The granules of a specific size range (4–5 mm) of LDPE, tiny spherical glass particles with a diameter of 106–600 µm and 0–50 µm with Sieve analysis

(UPV) testing was conducted to assess internal homogeneity and to validate the integrity of the hardened matrix. Figure 4 illustrates the comprehensive experimental workflow adopted in this study.

Wheatstone bridge

To connect strain gauges on a cube using the Wheatstone bridge method, the wiring and principle are as shown in the Figure 5 and 6, specifically tailored for strain gauge measurement on cubes [19].

Full Wheatstone Bridge equations:

1. Balanced Bridge condition (no strain applied):

$$\frac{R_1}{R_4} = \frac{R_2}{R_3} \tag{1}$$

When balanced, output voltage V_0 is:

$$V_0 = 0 \tag{2}$$

2. Output voltage of full Wheatstone Bridge with strain:

When strain causes changes Δ_{Ri} in each resistor Ri, the output voltage is:

$$V_0 = \frac{V_{ex}}{4} \times \left(\frac{\Delta R_1}{R_1} - \frac{\Delta R_2}{R_2} + \frac{\Delta R_3}{R_3} - \frac{\Delta R_4}{R_4}\right) \tag{3}$$

Table 2. Comprehensive concrete design mix

Materials (mass (1 m^3))	A	B	C	D	E	F	G	H	I	K
Portland cement	390	390	390	390	390	390	390	390	390	390
construction sand	897	807.3	762.42	717.6	807.3	807.3	807.3	897	897	897
coarse aggregate	914	914	914	914	868.3	822.6	776.9	868.3	822.6	776.9
Glass powder (GP) 0.106–0.6 mm	0	67.27	100.91	134.55	67.275	67.27	67.27	0	0	0
Ultra-fine glass powder (UFGP) 0.0–0.05 mm	0	22.42	33.67	44.85	22.42	22.42	22.42	0	0	0
polyethylene LDPE	0	0	0	0	45.7	91.4	137.1	45.7	91.4	137.1
Water	149	149	149	149	149	149	149	149	149	149
superplasticizer 1.4%	5.46	5.46	5.46	5.46	5.46	5.46	5.46	5.46	5.46	5.46
Percentage of (GP and UFGP) and LDPE content	0 % GP & UFGP. 0 % LDPE	10 % GP & UFGP. 0 % LDPE	15 % GP & UFGP. 0 % LDPE	20 % GP & UFGP. 0 % LDPE	10 % GP & UFGP. 5 % LDPE	10 % GP & UFGP. 10 % LDPE	10 % GP & UFGP. 15 % LDPE	0 % GP & UFGP. 5 % LDPE	0 % GP & UFGP. 10 % LDPE	0 % GP & UFGP. 5 % LDPE

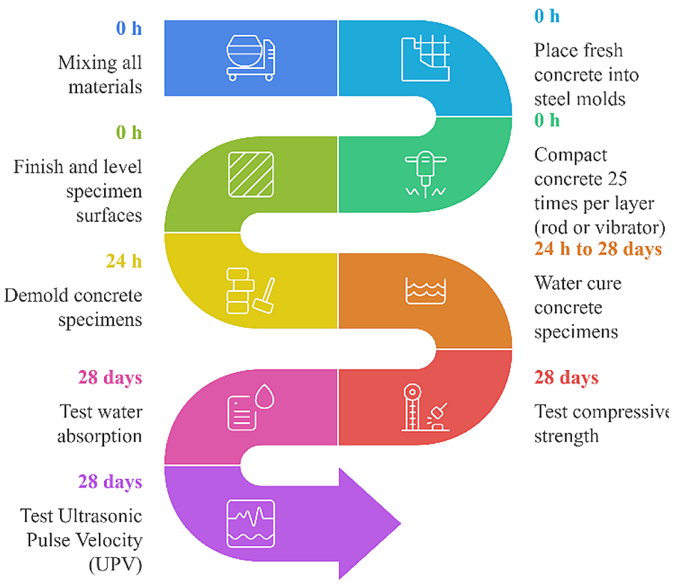

Figure 4. Mixing and casting and testing of all samples

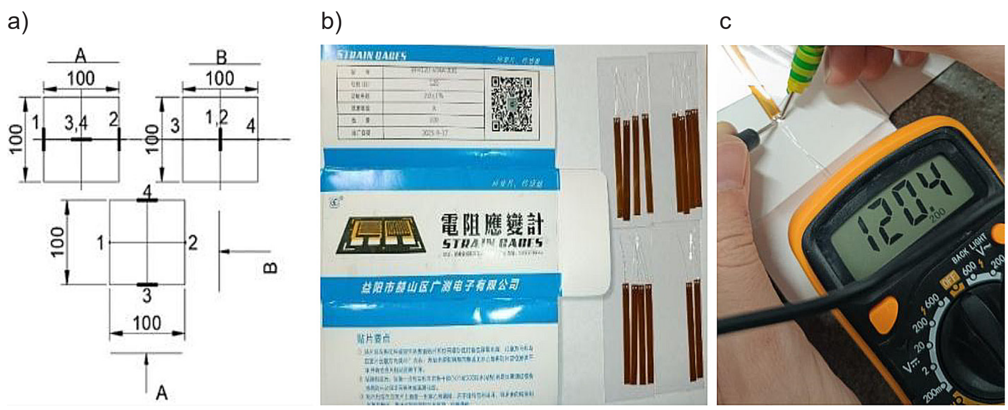

Figure 5. a) Scheme for gluing strain gauges onto cube samples, b) BX120-50AA 120-50AA Gauge concrete, c) PM830B high accuracy digital multimeter

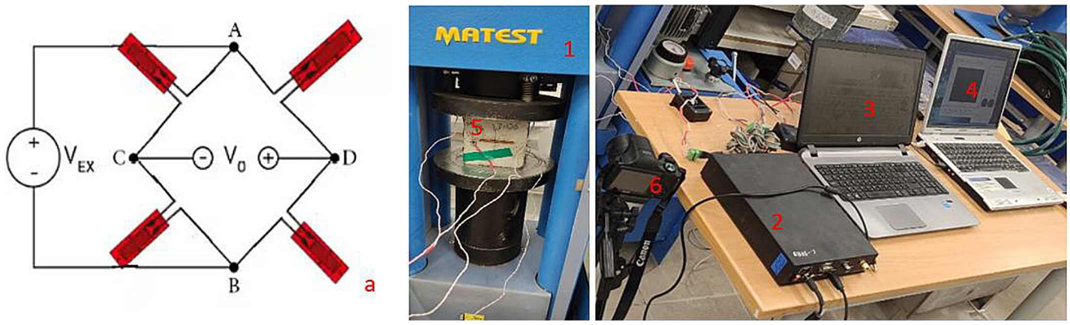

Figure 6. a) Full Wheatstone Bridge and b) 1) Matest hydraulic press, 2) Zetlab ZET 017-T8 strain gauge station, 3) personal computer for data processing (zetlab software), 4) personal computer for data processing (UTM2 software), 5) cube specimen (mix E) with BX120-50AA 120-50AA strain gauge, 6) Canon EOS 80D DSLR camera

3. Gauge factor and strain relation:

The relative change in resistance $\frac{\Delta R}{R}$ is related to mechanical strain ϵ by the gauge factor k

$$\frac{\Delta R_i}{R_i} = k \times \epsilon_i \quad (4)$$

Substituting this in:

$$V_0 = \frac{V_{ex}}{4} \times k \times (\epsilon_1 - \epsilon_2 + \epsilon_3 - \epsilon_4) \quad (5)$$

4. Simplified output voltage for symmetric strain:

If the strains are symmetric and balanced such that $(\epsilon_1 = \epsilon_3 = \epsilon \text{ and } \epsilon_2 = \epsilon_4 = -\epsilon$ (common in bending), then:

$$V_0 = \frac{V_{ex}}{4} \times k \times \big(\epsilon - (-\epsilon) + \epsilon - (-\epsilon)\big) = \\ = V_{ex} \times k \times \epsilon \quad (6)$$

Higher-order finite elements: Formulation and strain computation

Higher-order finite elements employ polynomial shape functions of degree p≥2 to approximate the solution field, distinguishing them from linear (first-order) elements which rely on straight-sided geometry and linear interpolation [20]. While the assembly of the stiffness matrix adheres to standard FEM procedures, it incorporates these higher-degree shape functions, typically defined by the addition of midside nodes. Within this framework, strains are calculated from displacement derivatives using the strain-displacement matrix, [B].

$$\begin{Bmatrix} \varepsilon_x \\ \varepsilon_y \\ \gamma_{xy} \end{Bmatrix} = \begin{bmatrix} \frac{\partial N}{\partial x} & 0 \\ 0 & \frac{\partial N}{\partial y} \\ \frac{\partial N}{\partial} & \frac{\partial N}{\partial x} \end{bmatrix} \begin{Bmatrix} u \\ v \end{Bmatrix} = [B]\{d\} \quad (7)$$

where: ε_x, ε_y – normal strains in x and y directions; γ_{xy} – shear strain ($\gamma_{xy} = 2\varepsilon_{xy}$;
$[B]$ – strain-displacement matrix;
$\{d\}$ – nodal displacement vector.

In higher-order elements, both the geometry and displacement fields are interpolated using identical shape functions defined within a natural coordinate system (ξ, η). Consequently, derivatives must be transformed from the element's natural coordinates to the global Cartesian system (x, y) [21]. This mapping is governed by the Jacobian matrix, [J]:

$$[J] = \begin{bmatrix} \frac{\partial x}{\partial \xi} & \frac{\partial y}{\partial \xi} \\ \frac{\partial x}{\partial \eta} & \frac{\partial y}{\partial \eta} \end{bmatrix} \quad (8)$$

where: x,y – global coordinates; ξ,η – natural coordinates.

Derivation of the transformation

The chain rule gives:

$$\begin{bmatrix} \frac{\partial \theta}{\partial \xi} \\ \frac{\partial \theta}{\partial \eta} \end{bmatrix} = [J] \begin{bmatrix} \frac{\partial \theta}{\partial x} \\ \frac{\partial \theta}{\partial y} \end{bmatrix} \rightarrow \begin{bmatrix} \frac{\partial \theta}{\partial x} \\ \frac{\partial \theta}{\partial y} \end{bmatrix} = [J]^{-1} \begin{bmatrix} \frac{\partial \theta}{\partial \xi} \\ \frac{\partial \theta}{\partial \eta} \end{bmatrix} \quad (9)$$

Solving for $[J]^{-1}$:

$$\frac{\partial\theta}{\partial x} = \frac{1}{[J]}\left(\frac{\partial y}{\partial \eta}\frac{\partial\theta}{\partial \xi} - \frac{\partial y}{\partial \xi}\frac{\partial\theta}{\partial \eta}\right) \tag{10}$$

$$\frac{\partial\theta}{\partial y} = \frac{1}{[J]}\left(\frac{\partial x}{\partial \xi}\frac{\partial\theta}{\partial \eta} - \frac{\partial x}{\partial \eta}\frac{\partial\theta}{\partial \xi}\right) \tag{11}$$

where:

$$[J] = det([J]) = \left(\frac{\partial x}{\partial \xi}\frac{\partial y}{\partial \eta} - \frac{\partial x}{\partial \eta}\frac{\partial y}{\partial \xi}\right) \tag{12}$$

This equation defines the strain-displacement relationship within the natural coordinate system for isoparametric higher-order finite elements. It serves as the theoretical basis for accurately computing strains in elements featuring curved geometries, such as cubic elements. The following analysis examines the significance of this relationship and its critical role in higher-order formulations.

$$\begin{Bmatrix} \partial_x \\ \partial_y \\ \gamma_{xy} \end{Bmatrix} = \frac{1}{[J]}\begin{bmatrix} \frac{\partial y}{\partial \eta}\frac{\partial\theta}{\partial \xi} - \frac{\partial y}{\partial \xi}\frac{\partial\theta}{\partial \eta} & 0 \\ 0 & \frac{\partial x}{\partial \xi}\frac{\partial\theta}{\partial \eta} - \frac{\partial x}{\partial \eta}\frac{\partial\theta}{\partial \xi} \\ \frac{\partial x}{\partial \xi}\frac{\partial\theta}{\partial \eta} - \frac{\partial x}{\partial \eta}\frac{\partial\theta}{\partial \xi} & \frac{\partial y}{\partial \eta}\frac{\partial\theta}{\partial \xi} - \frac{\partial y}{\partial \xi}\frac{\partial\theta}{\partial \eta} \end{bmatrix}\begin{Bmatrix} u \\ v \end{Bmatrix} \tag{13}$$

$$\{\partial\} = [D'][N]\{d\} \tag{14}$$

Formulate element matrix $[B]$ to evaluate $[k]$ such that $[B] = [D'][N]$

$$[B(\xi,\eta)] = \frac{1}{|[J]|}\left[|B_1|\right]\left[|B_2|\right]\ldots\ldots\left[|B_n|\right] \tag{15}$$

where: submatrices $[B]$ with index $i = 1$ to n number of nodes in the element are.

$$[B_i] = \frac{1}{|[J]|}\begin{bmatrix} \frac{\partial y}{\partial \eta}\frac{\partial(N_i)}{\partial \xi} - \frac{\partial y}{\partial \xi}\frac{\partial(N_i)}{\partial \eta} & 0 \\ 0 & \frac{\partial x}{\partial \xi}\frac{\partial(N_i)}{\partial \eta} - \frac{\partial x}{\partial \eta}\frac{\partial(N_i)}{\partial \xi} \\ \frac{\partial x}{\partial \xi}\frac{\partial(N_i)}{\partial \eta} - \frac{\partial x}{\partial \eta}\frac{\partial(N_i)}{\partial \xi} & \frac{\partial y}{\partial \eta}\frac{\partial(N_i)}{\partial \xi} - \frac{\partial y}{\partial \xi}\frac{\partial(N_i)}{\partial \eta} \end{bmatrix}\begin{Bmatrix} u \\ v \end{Bmatrix} \tag{16}$$

Stiffness matrix of an element with constant thickness h,

$$[K] = \iint_A [B]^T [D][B]h\,dx\,dy \tag{17}$$

Express the stiffness matrix in terms of ξ and η by general type of transformation

$$\iint_A f(x,y)h\,dx\,dy = \iint_A f(\xi,\eta)|J|h\,d\xi\,d\eta \tag{18}$$

After applying transformation equation, [k] can be written as

$$[K] = \int_{-1}^{1}\int_{-1}^{1}[B]^T [D][B]h|J|\,d\xi\,d\eta \tag{19}$$

Shape functions interpolate continuous fields from discrete nodal data in FEM [22]. Serendipity elements (Q8) use incomplete cubic polynomials to maximize efficiency without sacrificing accuracy [23,24]. Formulation in global coordinates (x,y) necessitates precise Jacobian-based transformations to handle arbitrary geometries.

$$\begin{aligned} x &= a_1 + a_2\xi + a_3\eta + a_4\xi\eta + a_5\xi^2 + \\ &+ a_6\eta^2 + a_7\xi^2\eta + a_8\xi\eta^2 \\ y &= a_9 + a_{10}\xi + a_{11}\eta + a_{12}\xi\eta + a_{13}\xi^2 + \\ &+ a_{14}\eta^2 + a_{15}\xi^2\eta + a_{16}\xi\eta^2 \end{aligned} \tag{20}$$

Shape functions:

$$\begin{aligned} N_1 &= \frac{1}{4}(1-\xi)(1-\eta)(-\xi-\eta-1) \\ N_2 &= \frac{1}{4}(1+\xi)(1-\eta)(\xi-\eta-1) \\ N_3 &= \frac{1}{4}(1+\xi)(1+\eta)(\xi+\eta-1) \\ N_4 &= \frac{1}{4}(1-\xi)(1+\eta)(-\xi+\eta-1) \\ N_5 &= \frac{1}{2}(1-\xi^2)(1-\eta) \\ N_6 &= \frac{1}{2}(1+\xi)(1-\eta^2) \\ N_7 &= \frac{1}{2}(1-\xi^2)(1+\eta) \\ N_8 &= \frac{1}{2}(1-\xi)(1+\eta^2) \end{aligned} \tag{21}$$

Concrete damaged plasticity (CDP) model

Concrete contains inherent micro-flaws (pores, micro-cracks) that act as initial damage, with macroscopic failure arising from their growth across scales [25]. The nonlinear stress-strain response and stiffness degradation result from micro-crack expansion coupled with plastic straining, necessitating an elastic-plastic damage framework [26]. In the CDP model, concrete is idealized as a homogeneous, isotropic continuum. Extending Lubliner et al., the formulation combines isotropic damage mechanics with distinct plasticity laws for tension and compression, capturing stiffness degradation under monotonic or cyclic loading and partial recovery upon unloading [27].

In elastic stage, the CDP model adopts the elastic model to describe the mechanical properties of materials. After stepping into the stage of damage, the relation between the elastic modulus in the CDP model can be described as.

$$E = (1 - d)E_0 \tag{22}$$

where: E_0 indicates the initial elastic modulus, d indicates the plastic-damage factor d_t or d_c in tension or compression and ranges from 0 to 1, in which 0 indicates that the material is not damaged and 1 indicates that the strength of the material is completely lost.

CDP model under single uniaxial tension/compression.

In Figure 7a, ε_{un} and σ_u denote the strain and stress at the unloading point, respectively, while ε_{0t}^{el} and ε_t^{el} represent the tensile elastic strain of undamaged and damaged concrete, respectively. The symbols ε_t^{pl} and ε_t^{ck} indicate the tensile plastic strain and tensile cracking strain of concrete, respectively.

The tensile damage data are input into Abaqus in the form $d_t - \varepsilon_t^{ck}$, and the program automatically converts the cracking strain into plastic strain using the following formula.

$$\varepsilon_t^{el} = \varepsilon_t^{ck} - \frac{d_t}{1 - d_t}\frac{\sigma_t}{E_0} \tag{23}$$

If the plastic strain ε_t^{pl} is negative or the cracking strain ε_t^{ck} is sufficiently small – indicating an intersection of the tensile unloading path – the Abaqus will show an error warning, as tensile damage cannot occur when ε_t^{pl} equals ε_t^{ck}. Regarding the compressive stress-strain curve, data points exceeding the elastic range will be treated as inelastic deformation.

The data is input into Abaqus as σ_c cversus ε_t^{in}. The compressive cracking strain is defined as the total strain minus the elastic strain calculated under undamaged material conditions, as illustrated in Figure 7b.

The data of the compressive damage will be entered into the finite element software (Abaqus) with the form of $d_c - \varepsilon_c^{in}$. Then, the program will automatically convert the cracking strain into plastic strain according to the following formula.

$$\varepsilon_c^{pl} = \varepsilon_c^{in} - \frac{d_c}{1 - d_c}\frac{\sigma_c}{E_0} \tag{24}$$

Finite element modeling in python

To support the experimental study, a custom FEM program, named CDP-FEM Studio, was developed in Python to simulate the behavior of concrete cube specimens containing GP, UFGP, and LDPE under uniaxial compression. The model employed a mapped hexahedral mesh to analyze stress distribution, displacement, and

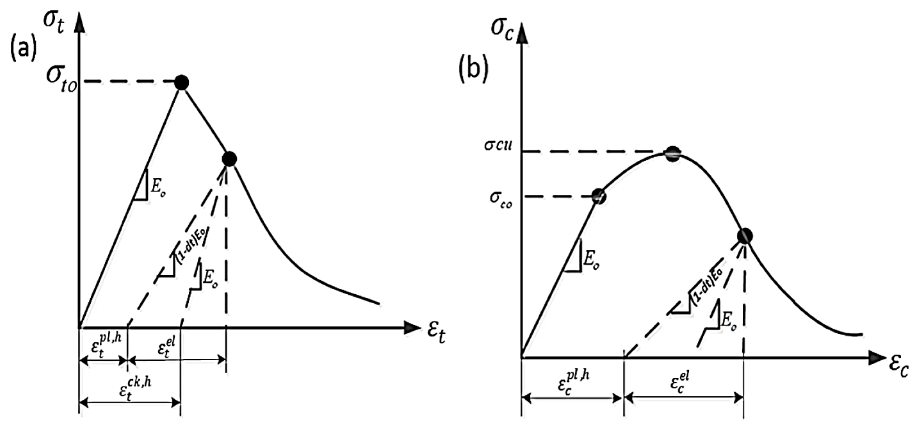

Figure 7. Concrete damaged plasticity (CDP) model response: (a) tensile and (b) compressive stress–strain behavior [28]

potential failure behavior. Material properties were assigned based on the 28-day experimental results. A linear elastic constitutive model was implemented in the analysis. The numerical results were validated by comparing the simulated load–displacement responses with both the experimental data and the results obtained from the SCAD++ software [29]. This Python-based FEM framework provided a simple and efficient alternative to commercial software for concrete cube compression analysis.

RESULTS AND DISCUSSION

Compressive strength at 28-day

The incorporation of GP and UFGP as partial replacements for fine aggregate, together with LDPE granules as partial replacements for coarse aggregate, offers a promising approach for improving both the mechanical performance and environmental sustainability of concrete. This study evaluated the 28-day compressive strength of ten different concrete mix designs (labeled A–K) to investigate the individual and combined effects of these sustainable materials, as presented in Table 3.

The concrete specimens were classified into four groups to evaluate the influence of the replacement materials on key engineering properties, including compressive strength, slump, modulus of elasticity, ultrasonic pulse velocity, water absorption, and density. Figures 8–13 illustrate the load–time curves (Figure 8), slump values (Figure 9), modulus of elasticity (Figure 10), ultrasonic pulse velocity (Figure 11), water absorption (Figure 12), and density (Figure 13) for all concrete mixtures.

- Group 1: Control mix without GP, UFGP, or LDPE replacement.

The control mix (A), containing 0% GP & UFGP and 0% LDPE replacement, achieved a reference compressive strength of 55.91 MPa

- Group 2: Concrete mixes incorporating GP and UFGP replacements without the inclusion of LDPE.

The highest compressive strength of 61.98 MPa was achieved with a 10% replacement of fine aggregate by GP & UFGP (Mix B), representing a 10.9% improvement over the control mix. This aligns with previous research [30], which identifies around 10% glass powder as the optimal replacement level. At this proportion, the pozzolanic activity of the glass powder enhances the pore structure and strengthens the interfacial transition zone without significantly weakening the cementitious matrix. However, increasing the glass powder content beyond 10% led to a gradual decrease in strength. Mix C (15% GP & UFGP) recorded 58.36 MPa, and Mix D (20% GP & UFGP) showed 55.95 MPa, roughly equivalent to the control. This trend suggests that the beneficial pozzolanic effects diminish when the replacement level exceeds the 10% threshold. On the other hand, Yan Diao [31] replaced cement and sand with glass powder and glass beads at 10%, 15%, and 20% levels, yielding compressive strengths of 33.5 MPa (0%), 28.2 MPa (10%), 31.1 MPa (15%), and 22.7 MPa (20%). In contrast, Al-Mashhadani [32] replaced cement with GP and achieved 48.4 MPa (0%), rising to 50.64 MPa (10%) and 49.25 MPa (15%), before dropping to 43.13 MPa (20%). However, Daban A. Muhedin [33] reported compressive strengths of sand replacement, 42 MPa (0%), 40 MPa (10%), 32 MPa (15%), and 28 MPa (20%); for cement replacement, 46 MPa (10%), 43 MPa (15%), and 36 MPa (20%). Overall, these results suggest that replacing sand with glass powder can be more effective than replacing cement, though outcomes vary by study.

- Group 3: Concrete mixes incorporating GP, UFGP, and LDPE replacements.

The interaction between 10% GP & UFGP and varying LDPE contents was tested in Mixes E, F, and G. Mix E (10% GP & UFGP + 5% LDPE) achieved 57.38 MPa, exceeding the control strength, showing low-volume plastic incorporation is feasible with optimized GP & UFGP. At this low dosage, spherical LDPE granules improve workability and packing, while GP & UFGP contribute pozzolanically to densification. However, higher LDPE contents caused strength degradation: Mix F (10% GP & UFGP + 10% LDPE) recorded 43.32 MPa, and Mix G (10% GP & UFGP + 15% LDPE) fell to 38.01 MPa. This reduction is due to LDPE's low elastic modulus, weak interfacial adhesion with cement paste, and increased trapped air from its hydrophobic nature. Mahesh's experimental [34] results for compressive strength at 10% glass powder replacement showed values of 18.9 MPa with 12% LDPE granules, 18.7 MPa at 18% LDPE, 18.7 MPa at 24% LDPE, and 18.3 MPa at 30% LDPE, indicating a slight decline in

Table 3. Statistical analysis results for all concrete samples

Sample	Compressive strength (Mpa)	(x̄)	(SD)	(CV)	Absorption %	(x̄)	(SD)	(CV)	Weight (g)	(x̄)	(SD)	(CV)
A1	55.95	55.92	0.12	0.21	0.7	0.80	0.09	11.18	2450.00	2457.80	7.36	0.30
A2	56.00				0.8				2460.50			
A3	55.75				0.9				2448.30			
A4	55.95				0.8				2459.20			
A5	56.05				0.7				2461.00			
A6	55.80				0.9				2467.80			
B1	62.15	61.98	0.22	0.35	0.6	0.66	0.05	7.47	2490.50	2497.96	4.09	0.16
B2	61.80				0.7				2498.20			
B3	62.00				0.6				2501.00			
B4	61.85				0.7				2496.80			
B5	62.30				0.7				2499.40			
B6	61.75				0.65				2501.86			
C1	58.50	58.37	0.16	0.28	0.50	0.59	0.07	11.23	2500.00	2505.14	3.21	0.13
C2	58.20				0.6				2506.50			
C3	58.40				0.6				2504.20			
C4	58.32				0.6				2507.80			
C5	58.19				0.7				2503.60			
C6	58.60				0.55				2508.74			
D1	56.10	55.96	0.18	0.32	0.8	0.81	0.06	7.23	2470.00	2475.48	3.48	0.14
D2	55.85				0.8				2474.60			
D3	55.90				0.85				2476.20			
D4	56.00				0.75				2478.50			
D5	55.70				0.9				2473.90			
D6	56.20				0.75				2479.68			
E1	57.50	57.38	0.16	0.29	0.5	0.54	0.05	9.08	2420.00	2425.95	4.21	0.17
E2	57.25				0.5				2426.80			
E3	57.40				0.6				2424.50			
E4	57.35				0.5				2428.10			
E5	57.15				0.6				2423.90			
E6	57.60				0.55				2432.40			
F1	43.50	43.32	0.19	0.44	0.6	0.65	0.05	8.43	2345.45	2348.87	2.20	0.09
F2	43.15				0.6				2348.25			
F3	43.30				0.7				2349.60			
F4	43.20				0.6				2350.10			
F5	43.15				0.7				2347.90			
F6	43.60				0.7				2351.90			
G1	38.20	38.01	0.22	0.57	0.8	0.70	0.08	11.07	2278.20	2282.00	2.75	0.12
G2	37.95				0.65				2280.80			
G3	38.00				0.65				2283.30			
G4	37.90				0.75				2284.70			
G5	37.70				0.6				2280.00			
G6	38.30				0.75				2285.00			

H1	46.05	45.86	0.20	0.43	0.8	0.85	0.04	5.26	2418.40	2421.86	2.12	0.09
H2	45.70				0.9				2420.90			
H3	45.90				0.8				2422.70			
H4	45.80				0.9				2424.10			
H5	45.60				0.85				2421.30			
H6	46.10				0.85				2423.76			
I1	38.95	38.75	0.22	0.57	0.85	0.91	0.06	6.44	2354.00	2357.50	2.05	0.09
I2	38.84				0.9				2356.80			
I3	38.70				0.95				2358.20			
I4	38.55				1				2359.50			
I5	38.45				0.85				2357.10			
I6	39.00				0.9				2359.40			
K1	29.30	29.17	0.17	0.59	0.95	1.03	0.06	5.86	2280.40	2283.18	1.93	0.08
K2	29.00				1.05				2282.70			
K3	29.20				1				2283.90			
K4	29.15				1.1				2284.60			
K5	28.95				1				2281.80			
K6	29.40				1.1				2285.68			

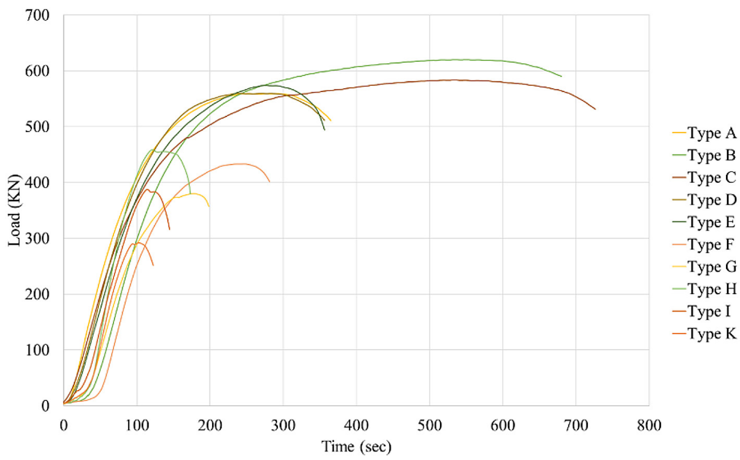

Figure 8. Load-time at 28-day

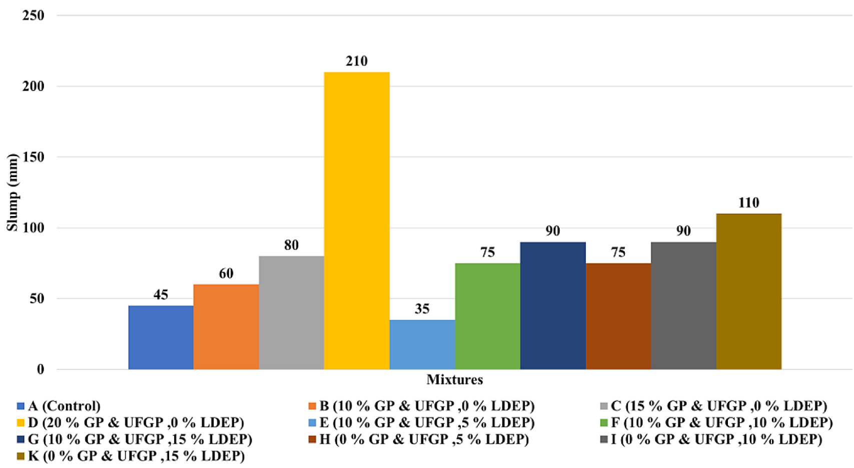

Figure 9. Slump test

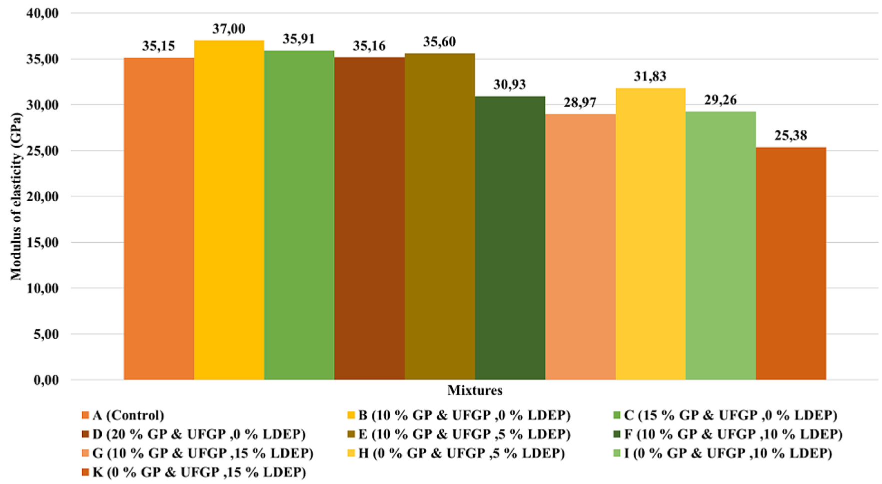

Figure 10. Modulus of elasticity (GPa)

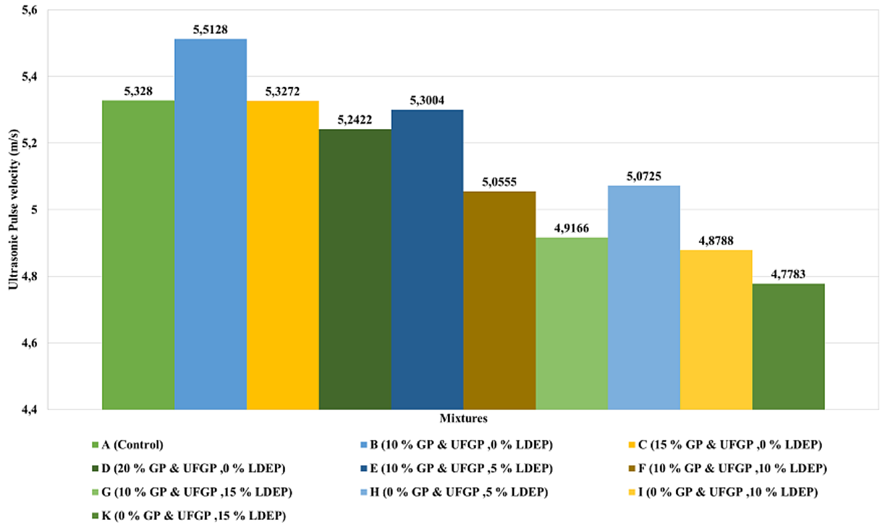

Figure 11. Ultrasonic pulse velocity (m/s)

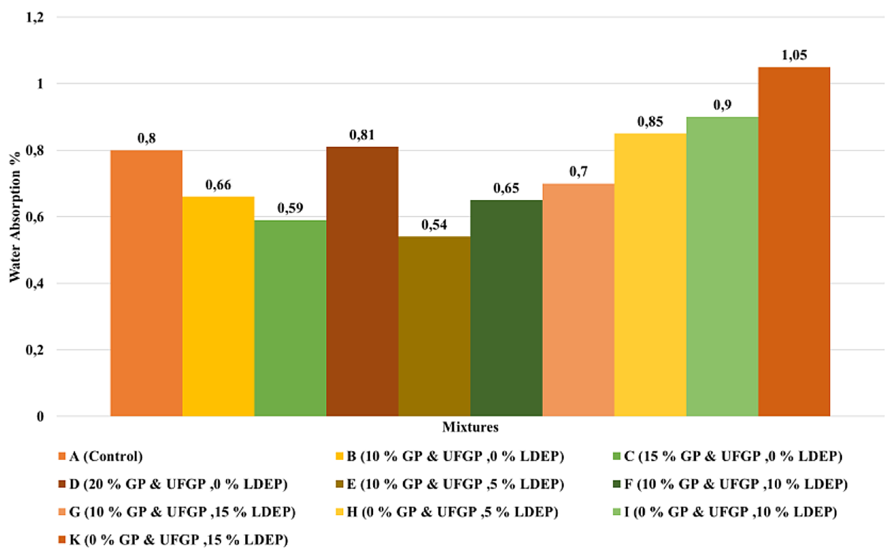

Figure 12. Water absorption %

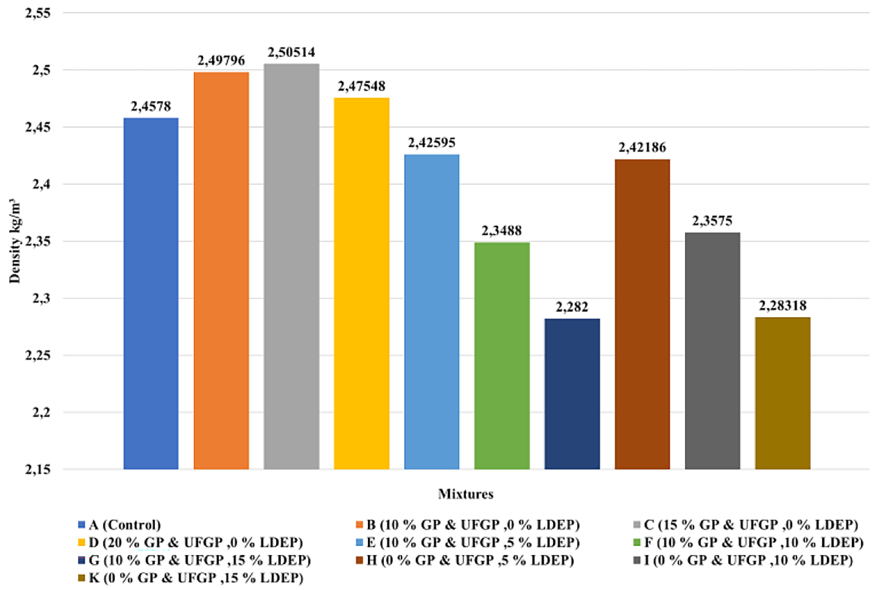

Figure 13. Density kg/m³

strength as LDPE content increased beyond 12%, with stability between 18% and 24%.

Group 4: Concrete mixes incorporating LDPE replacement without the inclusion of GP, UFGP.

Mixes H, I, and K incorporated LDPE granules without any GP & UFGP. At 5% replacement (Mix H), compressive strength was 45.85 MPa. This is approximately 18% below the control but remains potentially suitable for moderate-load or secondary structural applications. Strength declined to 38.75 MPa at 10% LDPE (Mix I) and dropped sharply to 29.16 MPa at 15% replacement (Mix K). This consistent inverse relationship between LDPE dosage and compressive capacity corroborates prior research [12], which indicates that plastic aggregate replacements beyond 10–15% typically reduce strength by more than one-third, primarily due to increased porosity and compromised load-transfer mechanisms at the aggregate–paste interface. On the other hand, Prakash [35] reported the compressive strengths of specimens with sand replaced by LDPE: 21.0 MPa at 0%, 19.89 MPa at 5%, and 18.7 MPa at 10%. Note that information regarding the 15% replacement level was not provided in the study. Vivek [36] observed a continuous decline in compressive strength when replacing sand with LDPE at varying percentages. Specifically, the reported compressive strengths were 27.33 MPa (0%), 15.67 MPa (5%), 13.0 MPa (10%), 10.67 MPa (15%), and 7.67 MPa (20%).

Slump test

Group 1: Control mix without GP, UFGP, or LDPE replacement.

The control mix A, which exhibited considerably lower initial workability (45 mm) compared to Al-Mashhadani's [32] control (150 mm).

Group 2: Concrete mixes incorporating GP and UFGP replacements without the inclusion of LDPE.

The inclusion of GP & UFGP significantly enhanced the slump, reaching 210 mm at the maximum dosage (Mix D). In contrast, Al-Mashhadani observed more moderate increases, with slump values rising from 161 mm to 178 mm when replacing cement with 10–20% glass powder. Furthermore, Ram [37] reported that replacing sand with glass powder resulted in slump values of 30 mm (0%), 45 mm (10%), 55 mm (15%), and 60 mm (20%). Ahmad [38] reported compressive strengths of 77 MPa, 85 MPa, and 100 MPa at 10%, 15%, and 20% cement replacement, respectively. In contrast, Khan [39] observed values of 99.06 MPa, 88.9 MPa, and 76.2 MPa at the same replacement levels. Meanwhile, Balasubramanian [40] reported strengths of 85 MPa, 90 MPa, and 98 MPa at 10%, 15%, and 20% cement replacement, respectively.

Group 3: Concrete mixes incorporating GP, UFGP, and LDPE replacements.

For Mix E (10% GP & UFGP + 5% LDPE granules), the slump exhibited a sharp decline to

35 mm, representing a 22% reduction compared to the control mix. For Mixes F and G, which contained higher plastic contents, the slump recovered to 75–90 mm. Mahesh observed that slump test results at 10% glass powder replacement decreased progressively with increasing LDPE granule content, from 91 mm at 12% LDPE to 87 mm at 18% LDPE, 83 mm at 24% LDPE, and 80 mm at 30% LDPE. While Balasubramanian reported slump values of 73 mm at 10% glass powder with 5% plastic, 69 mm at 10% glass powder with 10% plastic, and 58 mm at 10% glass powder with 15% plastic.

Group 4: Concrete mixes incorporating LDPE replacement without the inclusion of GP, UFGP.

Mix H (5% LDPE granules) exhibited a slump of 75 mm, Mix I (10% LDPE) achieved 90 mm, and Mix K (15% LDPE) recorded 110 mm, demonstrating progressive improvement in workability with increasing LDPE content. While Baboo [41] found that at 0%, 5%, 10%, and 15% replacement, the slump values were 80, 75, 58, and 45 mm, respectively.

Modulus of elasticity

Adding only GP & UFGP keep the concrete's stiffness relatively high. However, incorporating LDPE significantly reduces stiffness, especially when the content exceeds 10%. The modulus of elasticity remains high in mixes A–D (without LDPE), ranging between 35 and 37 GPa. Replacing sand with fine and ultrafine glass powder has only a minor effect on stiffness. In mixes B and E, stiffness slightly increases due to improved particle packing and a denser matrix. On the other hand, Ahmad reported modulus values of 20 GPa at 0%, 23 GPa at 15%, and 26 GPa at 20%, while Mohamed found values of 19.75 GPa at 0%, 20.62 GPa at 10%, 20.40 GPa at 15%, and 20.39 GPa at 20%.

When LDPE is introduced (mixes E–K), the modulus of elasticity decreases significantly because LDPE is more deformable than natural aggregate. This effect is further amplified by the reduction in coarse aggregate content, making the composite more flexible. The lowest modulus of elasticity is observed in mix K (25 GPa), which contains a high percentage of LDPE replacement.

Ultrasonic pulse velocity

Ultrasonic pulse velocity (UPV) changes for mixes A–K, which reflects concrete density, stiffness, and internal integrity. UPV is highest for the glass-modified mixes without LDPE (A–E), ranging from about 5.24 to 5.51 km/s, which indicates a dense, well-bonded matrix; mix B, with moderate glass replacement of sand, gives the maximum velocity, suggesting the best packing and lowest micro-void content. As LDPE is introduced (F–K), velocity gradually decreases from about 5.06 km/s in F to around 4.78 km/s in K, meaning the concrete becomes less dense and more heterogeneous because the soft, lightweight LDPE particles and reduced aggregate increase acoustic impedance mismatch and micro-voids. The small recovery at mix H (≈5.07 km/s) suggests that a low LDPE content without glass can still maintain relatively good internal quality, but further increases in LDPE (I, K) clearly reduce UPV, confirming that high polymer replacement impairs the continuity and compactness of the concrete.

Water absorption

The current study utilizing LDPE and quartz-based aggregates demonstrating superior overall moisture resistance compared to both Al-Mashhadani's HDPE-based research and Yassen's [42] glass powder-only investigation. The control mix in the present study recorded the lowest baseline absorption at 0.80%, substantially outperforming Al-Mashhadani's control (1.25%) and Yassen's (1.0351%), likely attributable to the high-purity quartz aggregates, optimized particle packing, and consistent superplasticizer dosage enhancing matrix density. All three studies confirm that glass powder incorporation progressively reduces water absorption through pore refinement and pozzolanic activity, yet the magnitude of improvement varies: the current study achieved absorption values of approximately 0.66%, 0.59%, and 0.62% at 10%, 15%, and 20% glass replacement respectively, compared to Yassen's 0.875%, 0.76%, and 0.72%, and Al-Mashhadani's 1.15%, 1.12%, and 1.05% at equivalent dosages, suggesting that the dual-fraction glass powder combined with well-graded quartz sand creates a more refined microstructure. Regarding plastic addition, LDPE-only mixes in the current study exhibited progressive absorption increases to 1.05% at 15% replacement, whereas Al-Mashhadani's HDPE mixes showed values rising from 1.28% to 1.39%, indicating that LDPE's lower density and smoother morphology may create fewer interconnected capillary pathways than angular HDPE particles. Most significantly, the hybrid Mix E (10% GP & UFGP + 5% LDPE) achieved the lowest absorption of 0.54% in the current study—substantially outperforming Al-Mashhadani's equivalent hybrid mix (10% glass + 5% HDPE: 1.13%) and Yassen's best glass-only result (20% glass: 0.72%)—demonstrating that the synergistic interaction between glass powder's pore-filling capacity and low-volume LDPE, when combined with high-quality quartz aggregates, can effectively mitigate the hydrophobic plastic's tendency to increase permeability. These comparative findings underscore that material selection—encompassing plastic type (LDPE vs. HDPE), glass particle fineness, aggregate mineralogy (quartz vs. conventional), and overall mixture proportions—critically governs water absorption performance, with the current quartz-based, LDPE-glass hybrid formulation offering a more durable, eco-friendly concrete solution for applications requiring enhanced resistance to moisture ingress and long-term durability in aggressive environments.

The control mix (A) exhibited a density of 2,4578 kg/m³, while mixes incorporating only GP & UFGP (B–D) showed a slight increase in density. Mix C showed the highest density at 2.505 kg/m³, which can be attributed to the higher density of GP & UFGP compared to natural sand. In contrast, mixes containing LDPE demonstrated a decrease in density with increasing plastic content. Mix G, which included the highest combined proportions of GP & UFGP and LDPE, showed the lowest density at 2.282 kg/m³, closely followed by Mix K (with the highest LDPE content alone) at 2.283 kg/m³. This reduction is primarily due to the significantly lower density of LDPE relative to conventional aggregates, resulting in a lighter composite material.

Mixes containing both GP & UFGP and a low amount of LDPE (E and F) had intermediate densities. This suggests that while GP & UFGP partly offset the drop in density, the LDPE has a stronger effect, leading to an overall lighter concrete. Such behavior is beneficial for applications requiring reduced dead load while maintaining adequate structural performance. On the other hand, Balasubramanian reported densities of 2.372 kg/m³, 2.385 kg/m³, 2.374 kg/m³, and 2.369 kg/m³ at 0%, 10%, 15%, and 20% glass powder replacement, respectively. For mixes incorporating both glass powder and plastic, densities of 2.368 kg/m³ at 10% glass powder with 5% plastic, 2,335 kg/m³ at 10% glass powder with 10% plastic, and 2.285 kg/m³ at 10% glass powder with 15% plastic were observed. While Sojobi [43] reported densities of 2.600, 2.550, 2.525, and 2.400 kg/m³ at 0%, 10%, 15%, and 20% LDPE replacement, respectively, Baboo [41] found that at replacement levels of 0%, 5%, 10%, and 15% plastic, the densities were 2.400, 2.350, 2.250, and 2.210 kg/m³, respectively.

The stress–strain curve for Mix E (Figure 14) illustrates both compressive and tensile behavior. Under compression, Mix E exhibits typical high-performance concrete behavior, with stress rising rapidly to a peak strength of about 57 MPa at a strain of approximately 0.00275. This high strength is notable given the inclusion of 45.7 kg/m³ of LDPE, suggesting that the addition of ~89.7 kg/m³ of glass powder compensates for potential strength loss (optimal mix). The glass powder likely acts as a micro-filler and contributes to pozzolanic reactions, improving the interfacial transition zone (ITZ) and maintaining matrix integrity. Beyond the peak, a softening branch indicates post-peak deformation.

In tension, Mix E shows a typical brittle response, with a linear elastic increase reaching a peak tensile strength of about 5.0 MPa, followed by a sudden drop due to crack initiation. The tensile-to-compressive strength ratio is

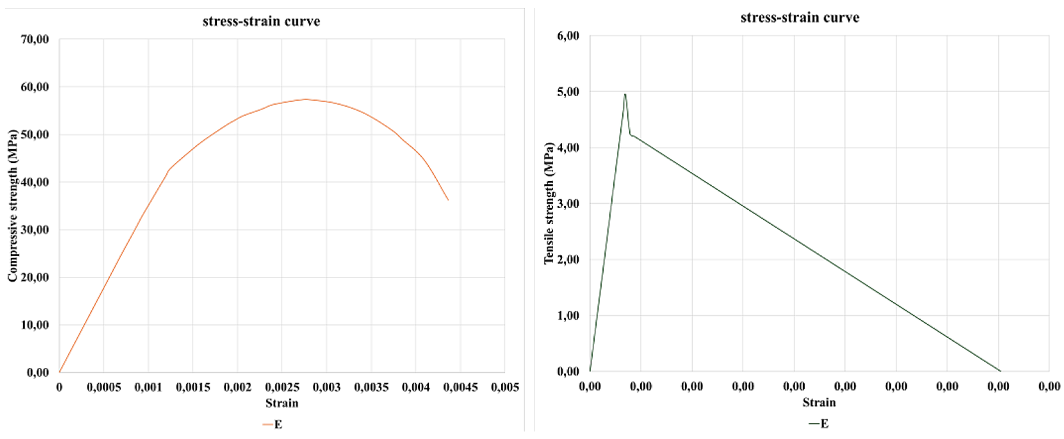

Figure 14. Stress-strain curve for sample E

approximately 1:11 to 1:12. While glass powder helps preserve compressive strength, the material remains brittle in tension. Overall, Mix E demonstrates that combining moderate amounts of glass powder with low LDPE content can produce durable concrete with high compressive capacity, suitable for structural applications where weight reduction and sustainability are desired.

Figure 15 illustrates the von Mises stress distribution in the cube specimen (Mix E) under compression, obtained through finite element simulation. The stress field shows a clear gradient, with lower stresses represented in blue and higher stresses in red, and most of the specimen experiencing a moderate level of stress relative to the peak values.

The highest stress shows up in the red-orange areas at the bottom corners and edges, where the specimen sits directly against the loading plate. Inside the cube, though, it's mostly blue – meaning the stress is spread pretty evenly. That tells us the material is fairly uniform and transfers load well, even with LDPE and GP & UFGP in the mix.

The CDP-FEM Studio program was used to calculate the displacement of the concrete specimen during loading using a FEM framework. The software provided numerical and graphical results for evaluating the deformation behavior under applied loads. A mesh and load-step convergence study was also conducted to examine the effect of mesh density on displacement predictions. The results showed that finer meshes improved the accuracy, stability, and convergence of the model, while coarser meshes

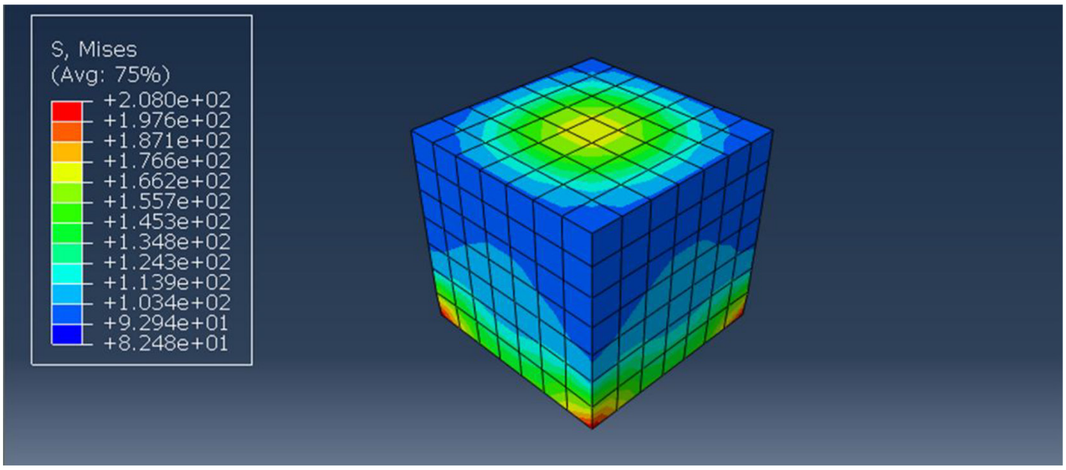

Figure 15. Von Mises stress distribution in a cube specimen (sample E)

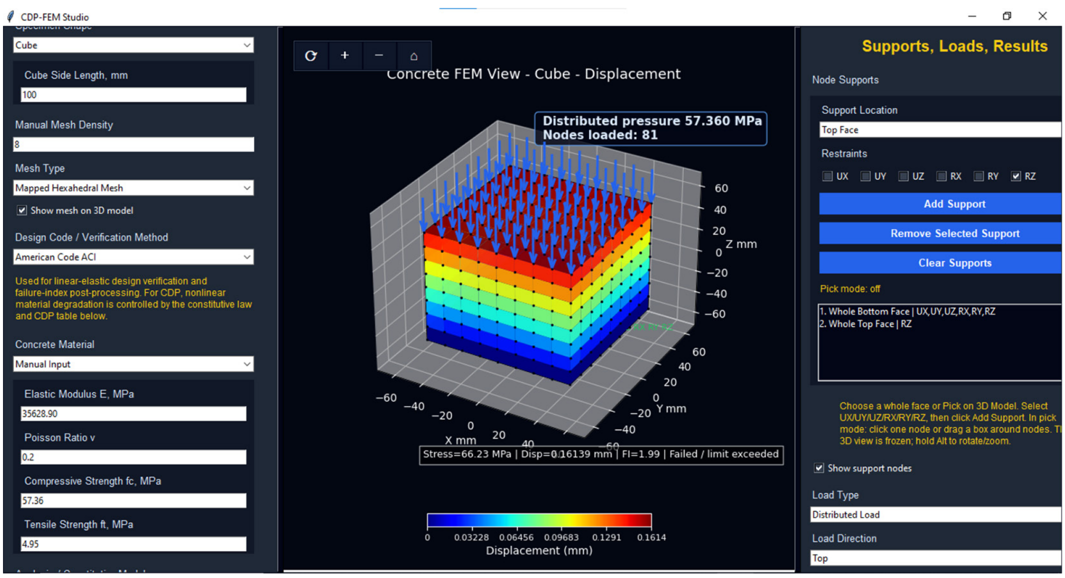

Figure 16. Interface of CDP-FEM Studio showing displacement in a cube specimen (sample E)

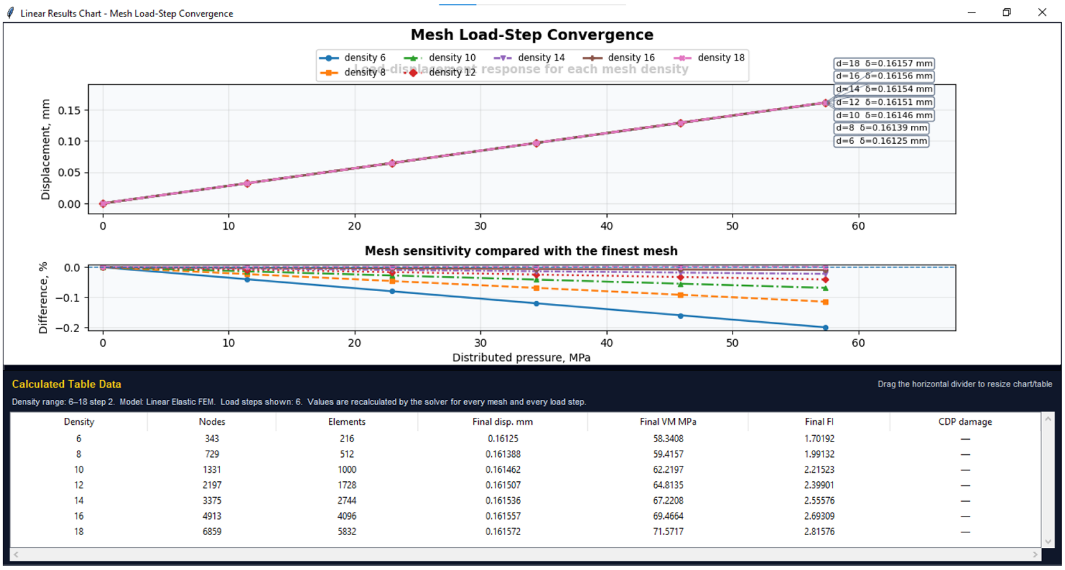

Figure 17. Mesh load-step convergence (displacement for sample E)

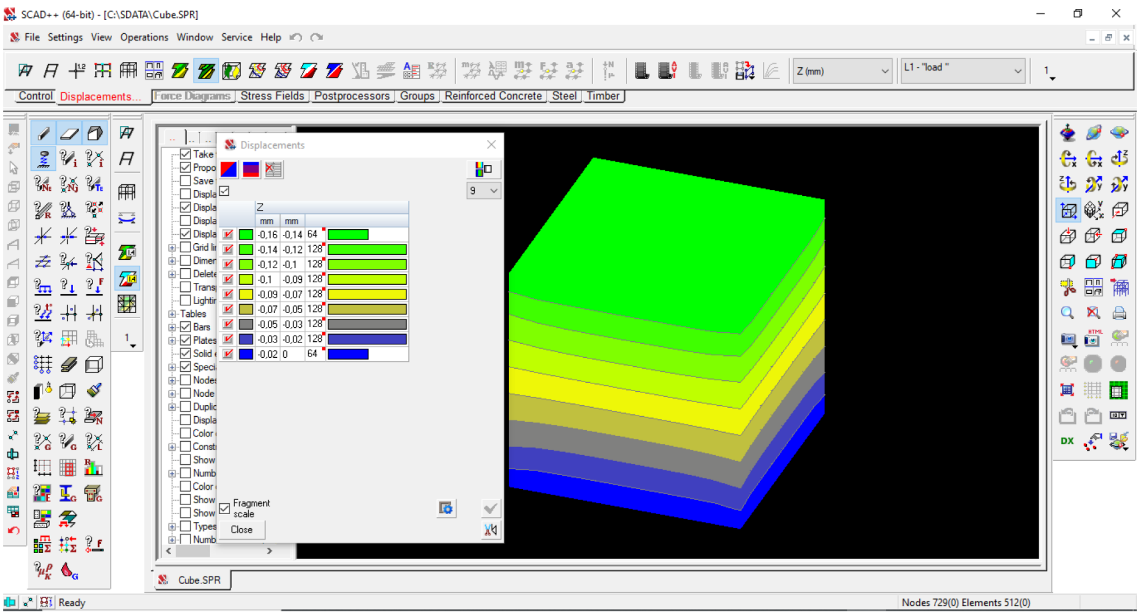

Figure 18. Interface of SCAD++ showing displacement in a cube specimen (sample E)

produced less accurate results. The study also helped determine an optimal mesh density that balanced simulation accuracy and computational efficiency. Figures (16–17) present the displacement results for concrete Sample E using different mesh densities. The results demonstrate the effect of mesh refinement on the predicted displacement behavior during loading. Figure 18 shows the displacement results obtained from the SCAD++ software for comparison and validation of the CDP-FEM Studio results.

The numerical displacement obtained using CDP-FEM Studio was 0.161572 mm, which showed very good agreement with the experimental displacement of 0.16132 mm and the numerical result obtained from the SCAD++ software as shown in the Figure 18, which was 0.16 mm.

CONCLUSIONS

This experimental investigation comprehensively evaluated the feasibility of integrating GP & UFGP and LDPE plastic waste into high-performance concrete formulations using quartz-based aggregates. The following conclusions are drawn:

- Optimal GP & UFGP replacement: The incorporation of 10% GP and UFGP as fine aggregate replacement (Mix B) yielded the maximum compressive strength of 61.98 MPa, demonstrating that GP and UFGP exhibit significant pozzolanic activity that refines the microstructure and strengthens the interfacial transition zone. Though 15% and 20% replacements still maintained strengths comparable to the control mix.
- The synergistic effect of hybrid replacement: Mix E, combining 10% GP and UFGP with 5% LDPE, achieved a compressive strength of 57.38 MPa—exceeding the control mix while reducing weight and attaining the lowest water absorption (0.54%), with a Von Mises stress distribution of 2.080×10^2, a maximum compressive strain of 0.00436, and a maximum tensile strain of 0.00160. This demonstrates that moderate GP & UFGP content can effectively mitigate the adverse effects of low-volume plastic aggregate incorporation through matrix densification and improved particle packing.
- LDPE content limitations: Higher LDPE replacement levels (>10%) resulted in pronounced strength degradation, with compressive strengths falling below 45 MPa. The hydrophobic nature, low elastic modulus, and weak interfacial bonding of LDPE particles increased porosity and compromised load-transfer mechanisms, limiting structural applicability at high replacement levels.
- Physical properties enhancement: GP and UFGP incorporation significantly improved workability (slump increased from 45 mm to 210 mm) and increased fresh density (up to 2505.14 g), while LDPE addition progressively reduced both stiffness (modulus decreased to 25 GPa) and ultrasonic pulse velocity (down to 4.78 km/s), confirming the lightweight, more compliant nature of plastic-modified concrete.
- Based on the comprehensive analysis of the ten tested concrete mixes (A–K), the optimal selection depends entirely on the specific performance requirements of the intended application. For applications demanding the highest compressive strength and elastic modulus—such as high-rise columns, heavy industrial flooring, or prestressed elements—Mix B is clearly superior, offering a peak strength of 61.98 MPa, the highest modulus at 37.00 GPa, and a low absorption of 0.66% with a workable 60 mm slump. If the priority is maximum durability and resistance to water ingress (e.g., water-retaining structures, foundations in wet soils, or bridge substructures), Mix E is the optimal choice, exhibiting the lowest absorption rate of just 0.54% while still maintaining a very good strength of 57.38 MPa and moderate stiffness. For situations requiring excellent workability to fill congested reinforcement or complex formwork (e.g., heavily reinforced beams or columns), Mix D is the best fit, providing an exceptionally high slump of 210 mm (self-compacting range) with acceptable strength (55.96 MPa) and durability (0.81% absorption). Finally, for a balanced general-purpose structural concrete combining good strength, reasonable workability, and low absorption without extreme values in any property, Mix C (58.37 MPa, 80 mm slump, 0.59% absorption) offers the most versatile and robust performance. Mixes F, G, H, I, and K exhibit significantly lower compressive strengths (29–46 MPa) and are only suitable for low-strength, non-critical applications such as temporary works, backfill, or lightweight non-structural elements.
- Confirmation that the Python-based CDP-FEM Studio accurately predicted the displacement behavior of concrete cube specimens under compression, with a numerical displacement of 0.161572 mm compared to the experimental value of 0.16132 mm and the SCAD++ result of 0.16 mm, demonstrating excellent agreement and reliability.

REFERENCES

1. Yang, B., Liu, Y. and Wang, X.Y. A hydration model to evaluate the properties of cement–quartz powder hybrid concrete. materials, 2024; 17. https://doi.org/10.3390/ma17112769
2. Tavares, L.R.C., Junior, J.F.T., Costa, L.M., da Silva Bezerra, A.C., Cetlin, P.R. and Aguilar, M.T.P. Influence of quartz powder and silica fume on the performance of Portland cement. Scientific Reports, Nature Research, 2020; 10. https://doi.org/10.1038/s41598-020-78567-w
3. Fedosov, S. V., Aleksandrova, O. V., Bulgakov, B.I., Lukyanova, N.A. and Duc Vinh, Q.N.

Corrosion-resistant concretes for coastal underground structures. Magazine of Civil Engineering, 2024; 17. https://doi.org/10.34910/MCE.126.6

4. Sergey Fedosov, O.A.N.D.V.Q.B.B. and N.G. Use of white quartz sand as fine aggregate in concrete for hydraulic structures. Proceedings of FORM 2022.
5. Faisal, F., Sutandar, E. and Supriyadi, A. The effects of quartz sand variation as an additive on concrete compressive strength (no air added). Jurnal Teknik Sipil, 2025; 25, 2442–2456. https://doi.org/10.26418/jts.v25i4.92086
6. Sivasuriyan, A. and Koda, E. Incorporation of waste glass powder in the sustainable development of concrete. Materials, 2025, July 1. https://doi.org/10.3390/ma18143223
7. Lam, W.L., Cai, Y., Sun, K., Shen, P. and Poon, C.S. Roles of ultra-fine waste glass powder in early hydration of Portland cement: hydration kinetics, mechanical performance, and microstructure. Construction and Building Materials, 2024; 415. https://doi.org/10.1016/j.conbuildmat.2024.135042
8. Ayub, T., Jamil, T., Ayub, A., Khan, A.U.R., Mehmood, E. and Sheikh, M.D. Effect of glass powder on the compressive strength and drying shrinkage behavior of OPC- and LC3-50-based cementitious composites of various strengths. Advances in Materials Science and Engineering, 2024. https://doi.org/10.1155/2024/8860083
9. Ul Haq, M.Z., Singh, S., Vora, T., Ak, D., Tomar, A., S, V., Das, P., Thirugnanasambandam, A. and Kumar, V.V. Sustainable concrete mix optimization with recycled glass powder and nano-silica: a Taguchi method analysis. Journal of Structural Integrity and Maintenance, 2026; 11. https://doi.org/10.1080/24705314.2025.2546210
10. Mohammed, Z.M. Behavior of Sustainable Reactive Powder Concrete by Using Glass Powder as a Replacement of Cement. IOP Conference Series: Earth and Environmental Science, IOP Publishing Ltd. 2022. https://doi.org/10.1088/1755-1315/961/1/012022
11. Lam, W.L., Cai, Y., Sun, K., Shen, P. and Poon, C.S. Roles of ultra-fine waste glass powder in early hydration of Portland cement: Hydration kinetics, mechanical performance, and microstructure. Construction and Building Materials, 2024; 415. https://doi.org/10.1016/j.conbuildmat.2024.135042
12. Obeid, M., Abu-Mahadi, M. and Nasrat, N.A. Mechanical and microstructural behavior of concrete with LDPE waste as partial fine aggregate replacement. Bulletin of Belgorod State Technological University named after. V. G. Shukhov, 2026; 11, 21–31. https://doi.org/10.34031/2071-7318-2026-11-3-21-31
13. Ahmad, S.S.E., Graf, A.A.A.A. and Bneni, M.K. Mechanical performance of sustainable concrete containing industrial waste admixtures of SF, FA, CCI, and crushed quartz at different water-binder ratios. Scientific reports, 2026; 16, 3055. https://doi.org/10.1038/s41598-025-34612-0
14. Sabih, G., Tarefder, R.A. and Jamil, S.M. Optimization of gradation and fineness modulus of naturally fine sands for improved performance as fine aggregate in concrete. Procedia Engineering, 2016; 66–73. https://doi.org/10.1016/j.proeng.2016.04.016
15. Vivek, S., Hari Krishna, P. and Gunneswara Rao, T.D. A Study on the mechanical behavior of concrete made with partial replacement of fine aggregate with waste plastic (LDPE). Materials Today: Proceedings, Elsevier Ltd. 2023. https://doi.org/10.1016/j.matpr.2023.04.059
16. Oti, J., Adeleke, B.O., Rathnayake, M., Kinuthia, J.M. and Ekwulo, E. Strength and durability characterization of structural concrete made of recycled plastic. Materials, 2024; 17. https://doi.org/10.3390/ma17081841
17. Ministry of energy and Mineral Resources. Mineral Resources in Jordan. https://memr.gov.jo/EBV4.0/Root_Storage/EN/Project/Mineral_Resources_in_Jordan.pdf
18. Batholith. Fractionated Quartz Sand. Chemical Composition. http://www.batolit.ru/93_p.shtml.
19. Lizon, B. and Wu, J. (2024) A Basic Guide to Bridge Measurements. www.ti.com
20. Resmy, V.R. and Rajasekaran, C. (2024) Topology optimization of concrete beam using higher order finite elements. Lecture Notes in Civil Engineering, 113–123. https://doi.org/10.1007/978-981-97-4844-0_10
21. Alexander V. Panfilov., Kirsten H.W.J.ten Tusscher and Rob J. de Boer. Matrices, linearization, and the Jacobi matrix. Theoretical Biology, 2025. https://tbb.bio.uu.nl/rdb/books/math.pdf#page=9.20
22. Nguyen, D.D., Nguyen, M.N. and Bui, T.Q. Polygonal elements with Richardson-extrapolation based numerical integration schemes for hyperelastic large deformation analysis. Computers and Structures, 2025; 309. https://doi.org/10.1016/j.compstruc.2025.107654
23. Soh, A.-K., Yuqiu, L. and Song, C. Development of eight-node quadrilateral membrane elements using the area coordinates method. Computational Mechanics, 25, 376–384. https://doi.org/https://doi.org/10.1007/s004660050484
24. Kikuchi, F., Okabe, M. and Fujio, H. Modifcation of the 8-node serendipity element. Computer Methods in Applied Mechanics and Engineering, 1998; 179, 91–109. https://doi.org/https://doi.org/10.1016/S0045-7825(99)00031-6
25. J. Stauffer, C. Woodward and K. White. Nonlinear ultrasonic testing with resonant and pulse velocity parameters for early damage in concrete. Aci Materials Journal, 2005; 102, 118–121.

26. Xiao, Y., Chen, Z., Zhou, J., Leng, Y. and Xia, R. Concrete plastic-damage factor for finite element analysis: concept, simulation, and experiment. Advances in Mechanical Engineering, 2017; 9, 1–10. https://doi.org/10.1177/1687814017719642
27. Altaee, M., Kadhim, M., Altayee, S. and Adheem, A. (2020) Employment of damage plasticity constitutive model for concrete members subjected to high strain-rate. European Alliance for Innovation n.o. https://doi.org/10.4108/eai.28-6-2020.2298164
28. Alasadi, S., Ibrahim, Z., Shafigh, P., Javanmardi, A. and Nouri, K. An Experimental and numerical study on the flexural performance of over-reinforced concrete beam strengthening with bolted-compression steel plates: Part II. Applied Sciences (Switzerland), 2020; 10. https://doi.org/10.3390/app10010094
29. SCAD Structure. Structure CAD Office – an Integrated Software System for Structural Analysis and Design.
30. Rodrigues de Brito, B., Bacurau Martins, A.B., Da Silva magalhães, R., Fernando dos Santos, L., Tadeu de Almeida Santos, G., Augusto Junior, J., Rainho Teixeira, S. and Eunice de Souza, A. Glass powder from non-returnable bottles: Pozzolanic additive to mortar. Engineering & Technology Scientific Journal, 2022; 1. https://doi.org/10.55977/etsjournal.v01i01.e022003
31. Diao, Y., Chen, L. and Huang, Y. Experimental study on mechanical properties of concrete containing waste glass and its application on concrete-filled steel tubular columns. Processes, 2023; 11. https://doi.org/10.3390/pr11040975
32. Duraid Ali Jasim, A.M., Sing Wong, L., Midhin, M.A.K. and Chyad Liejy, M. Evaluating high performance concrete properties partially replacing waste glass powder WGP and waste high density polyethylene (HDPE) beads. Indian Journal of Engineering, 2025; 22. https://doi.org/10.54905/disssi.v22i57.e2ije1691
33. Muhedin, D.A. and Ibrahim, R.K. Effect of Waste Glass Powder as Partial Replacement of Cement & Sand in Concrete. Case Studies in Construction Materials, 2023; 19. https://doi.org/10.1016/j.cscm.2023.e02512
34. Paliwal, M.C. and Kushwaha, S.S. Analysis of mechanical properties of concrete using plastic granules as coarse aggregates. Journal of Information Systems Engineering and Management, 2024; 2025, 2468–4376. https://www.jisem-journal.com/
35. Noriya, P. and Dwivedi, P. Experimental investigation of concrete utilizing plastic waste HDPE and Ldpe as an replacement of aggregate in concrete. International Journal of All Research Education and Scientific Methods, 2021; 9, 2455–6211.
36. Vivek, S., Hari Krishna, P. and Gunneswara Rao, T.D. A study on the mechanical behavior of concrete made with partial replacement of fine aggregate with waste plastic (LDPE). Materials Today: Proceedings, Elsevier Ltd. 2023. https://doi.org/10.1016/j.matpr.2023.04.059
37. Bahadur, R. and Kumar Parashar, A. An Investigation of Waste Glass Powder with the Substitution of Sand on Concrete Mix. Materials Today: Proceedings, Elsevier Ltd. 2023. https://doi.org/10.1016/j.matpr.2023.02.123
38. Ahmad, J., Martinez-Garcia, R., Algarni, S., de-Prado-Gil, J., Alqahtani, T. and Irshad, K. Characteristics of sustainable concrete with partial substitutions of glass waste as a binder material. International Journal of Concrete Structures and Materials, Springer Nature Korea, 2022; 16. https://doi.org/10.1186/s40069-022-00511-1
39. Khan, F.A., Shahzada, K., Ullah, Q.S., Fahim, M., Khan, S.W. and Badrashi, Y.I. Development of environment-friendly concrete through partial addition of waste glass powder (Wgp) as cement replacement. Civil Engineering Journal (Iran), Salehan Institute of Higher Education, 2020; 6, 2332–2343. https://doi.org/10.28991/cej-2020-03091620
40. Balasubramanian, B., Gopala Krishna, G.V.T., Saraswathy, V. and Srinivasan, K. Experimental Investigation on Concrete Partially Replaced with Waste Glass Powder and Waste E-Plastic. Construction and Building Materials, 2021; 278. https://doi.org/10.1016/j.conbuildmat.2021.122400
41. Rai, B., Rushad, S.T., Kr, B. and Duggal, S.K. Study of waste plastic mix concrete with plasticizer. ISRN Civil Engineering, 2012, 1–5. https://doi.org/10.5402/2012/469272
42. Yassin, M.M., Mahmoud, A.S. and Hama, S.M. Effectiveness of Glass Wastes as Powder on Some Hardened Properties of Concrete. Al-Nahrain Journal for Engineering Sciences, Al-Nahrain Journal for Engineering Sciences, 2019; 22, 14–17. https://doi.org/10.29194/njes.22010014
43. Sojobi, A.O. and Owamahand, H.I. Evaluation of the suitability of low-density polyethylene (LDPE) waste as fine aggregate in concrete. Nigerian Journal of Technology, 2014; 33. https://doi.org/http://dx.doi.org/10.4314/njt.v33i4.1